

Zero-Shot Scene Change Detection

Kyusik Cho¹, Dong Yeop Kim^{2,1}, Euntai Kim^{1*}

¹Yonsei University, Seoul, Republic of Korea

²Korea Electronics Technology Institute, Seoul, Republic of Korea
ks.cho@yonsei.ac.kr, sword32@keti.re.kr, etkim@yonsei.ac.kr

Abstract

We present a novel, training-free approach to scene change detection. Our method leverages tracking models, which inherently perform change detection between consecutive frames of video by identifying common objects and detecting new or missing objects. Specifically, our method takes advantage of the change detection effect of the tracking model by inputting reference and query images instead of consecutive frames. Furthermore, we focus on the content gap and style gap between two input images in change detection, and address both issues by proposing adaptive content threshold and style bridging layers, respectively. Finally, we extend our approach to video, leveraging rich temporal information to enhance the performance of scene change detection. We compare our approach and baseline through various experiments. While existing train-based baseline tend to specialize only in the trained domain, our method shows consistent performance across various domains, proving the competitiveness of our approach.

Code — <https://github.com/kyusik-cho/ZSSCD>

Introduction

Scene Change Detection (SCD) is the task that aims to detect differences between two scenes separated by a temporal interval. Recently, SCD has gained significant interest in various applications involving mobile drones and robots. For instance, drone-based SCD has been studied for land terrain monitoring (Lv et al. 2023; Song et al. 2019; Agarwal, Kumar, and Singh 2019), construction progress monitoring (Han et al. 2021), and urban feature monitoring (Chen et al. 2016). Additionally, SCD using mobile robots has also been researched for natural disaster damage assessment (Sakurada and Okatani 2015; Sakurada, Okatani, and Deguchi 2013), urban landscape monitoring (Alcantarilla et al. 2018; Sakurada, Shibuya, and Wang 2020), and industrial warehouse management (Park et al. 2021, 2022).

Recently, SCD has been tackled using deep learning. Deep learning-based SCD techniques follow a procedure of learning from a training dataset and applying the model to a test dataset. These approaches tend to face two main challenges: dataset generation costs and susceptibility to style

variations. Firstly, creating a training dataset for SCD models is labor-intensive and costly. Recent research has focused on reducing these costs through semi-supervised (Lee and Kim 2024; Sun et al. 2022) and self-supervised learning (Seo et al. 2023; Furukawa et al. 2020) methods, as well as the use of synthetic data (Sachdeva and Zisserman 2023; Lee and Kim 2024). While these approaches mitigate the expense of labeling, they often overlook the cost of acquiring image pairs, which arises from the substantial temporal intervals to capture changes. Secondly, due to the substantial temporal intervals between pre-change and post-change images, variations in seasons, weather, and time introduce significant differences in their visual characteristics. Consequently, SCD techniques must be robust to these style variations to be effective. However, the training dataset cannot include all the style variations present in real-world scenarios, making the trained model vulnerable to style variations that are not included in the training set.

To address these problems, we propose a novel training-free zero-shot SCD method. Our method does not require a training dataset, thereby eliminating collection costs and allows it to be applied to any problem with arbitrary styles. To the best of our knowledge, this paper is the first to attempt zero-shot SCD without training on SCD datasets. The key idea of this paper is to formulate SCD as a tracking problem, and apply a foundation tracking model to conduct zero-shot SCD. This idea stems from the observation that the tracking task is fundamentally similar to change detection. Specifically, tracking models (Cheng et al. 2023a; Cheng and Schwing 2022) maintain or build tracks by identifying the same objects, disappeared objects, and newly appeared objects in two consecutive images, even when the camera and objects move. Thus, if the two consecutive images in tracking are replaced with the two images before and after the change in SCD, the tracking model can automatically solve SCD without training.

However, there are some differences between tracking and SCD tasks: (a) Unlike tracking, the two images before and after the change in SCD might have different styles due to a large time gap between two images. We refer to this SCD trait as the style gap. (b) Objects change very little between two consecutive images in tracking, whereas objects change abruptly in SCD. We refer to this SCD trait as the content gap. To address these issues in our zero-shot SCD

*Corresponding author.

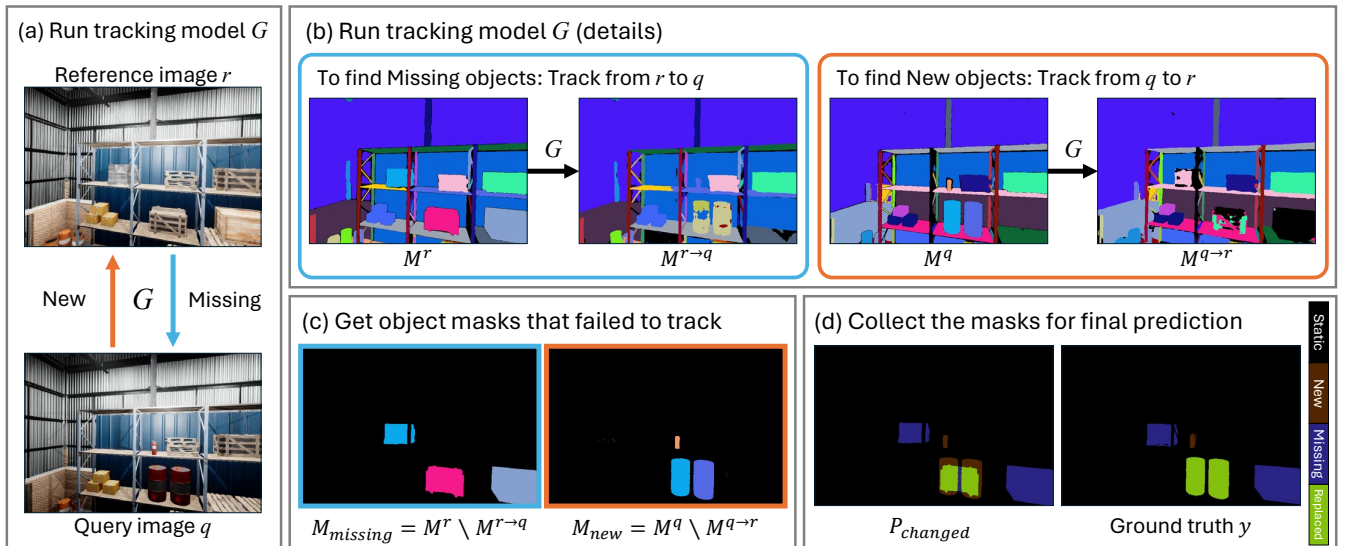


Figure 1: **The basic idea of SCD with tracking model.** (a) We execute the tracking model G with r and q . (b) We denote the tracking result from r to q as $M^{r \rightarrow q} = G(r, q, M^r)$, and the tracking result from q to r as $M^{q \rightarrow r} = G(q, r, M^q)$. (c) ‘Missing’ objects are the objects that exist in r but not in q . Therefore, we compare M^r and $M^{r \rightarrow q}$ to find missing objects. Conversely, ‘new’ objects are identified by comparing M^q and $M^{q \rightarrow r}$. (d) The final prediction is the simple combination of new and missing.

method, we introduce a style bridging layer and a content threshold, respectively.

Finally, we extend our approach to sequence, to introduce the zero-shot SCD approach works on the video. Since our approach operates based on a tracking model, it can be seamlessly extended to work with video sequences. The proposed zero-shot SCD approach has been evaluated on three benchmark datasets and demonstrated comparable or even superior performance compared to previous state-of-the-art training-based SCD methods.

Related Work

Scene Change Detection (SCD) In recent years, numerous deep learning-based change detection methods have been proposed for SCD. DR-TANet (Chen, Yang, and Stiefelhagen 2021) utilized attention mechanism based on the encoder-decoder architecture. SimSaC (Park et al. 2022) developed a network with a warping module to correct distortions between images. C-3PO (Wang, Gao, and Wang 2023) developed a network that fuses temporal features to distinguish three change types. However, various studies have aimed to address the challenge of obtaining data. For instance, Lee and Kim (2024) and Sun et al. (2022) have introduced semi-supervised learning, while Seo et al. (2023) and Fukawa et al. (2020) proposed the self-supervised learning with unlabeled data. However, Sachdeva and Zisserman (2023) and Lee and Kim (2024) utilized synthetic data to effectively increase the dataset. Despite these methods effectively reducing the label costs, they tend to overlook the cost of collecting image pairs. Moreover, the robustness against style change has not been previously discussed. An effective SCD method should be able to focus on content

changes regardless of variations in image style. However, since a single dataset cannot encompass all possible style variations, the performance tends to be specialized for the styles present in the dataset. This issue, while not evident in controlled laboratory environments, becomes a significant problem in real-world applications. Therefore, we propose a novel SCD method that does not rely on datasets. Our method operates without a training dataset, thus ensuring independence from specific styles.

Segmenting and Tracking Anything Recently, Segment Anything (Kirillov et al. 2023) has demonstrated highly effective performance in universal image segmentation. SAM has shown the ability to perform various zero-shot tasks, and has served as the foundational model for various studies (Peng et al. 2023; Maquiling et al. 2024). Building upon this research, researchers have explored various methods to extend its application to tracking. For example, SAM-Track (Cheng et al. 2023b) implemented tracking by combining SAM with the DeAOT (Yang and Yang 2022) mask tracker. SAM-PT (Rajič et al. 2023) integrated SAM with point tracking to develop the pipeline. DEVA (Cheng et al. 2023a) proposed a pipeline that uses the XMem tracker (Cheng and Schwing 2022) to track provided masks without additional training. Among various studies, we adopted DEVA with SAM masks as our tracking model, to achieve track-anything for SCD without further training.

Method

Each datum for scene change detection (SCD) is represented as a triplet (r, q, y) , where r and q denote paired images acquired at distinct times t_0 and t_1 , respectively, and y represents the change label between the image pair. The primary

objective of this task is to discern the scene change between the images captured at t_0 and t_1 when inspecting the latter. Herein, we call the image obtained at t_0 (r) as the reference image and the image acquired at t_1 (q) as the query image.

To perform scene change detection without training, our methodology integrates two pretrained models: a segmentation model F and a tracking model G . The segmentation model F segments images in an unsupervised manner, while the tracking model G tracks each mask generated by F across multiple images. We employ the Segment Anything Model (SAM) (Kirillov et al. 2023) as the segmentation model F and DEVA (Cheng et al. 2023a) for the tracking model G . Comprehensive details about parameters for F and G , and details about the mask generation process are provided in the supplementary materials.

The rest of the Method section is structured as follows: First, we introduce the basic idea for performing SCD between two images using F and G . Next, we discuss the differences between the tracking task and the SCD task, and then introduce methods to overcome these differences. Finally, we extend our approach to the video level.

Scene Change Detection with Tracking Model

Our approach uses two pretrained models, a segmentation model F and a tracking model G . The segmentation model F partitions image I into object-level masks, forming the set $M = \{m_1, m_2, \dots, m_n\}$. There exists no overlap between distinct masks, that is, $m_i \cap m_j = 0, \forall i \neq j$. The tracking model G takes consecutive frame images (I^0, I^1) and the object masks of the first frame $M^0 = F(I^0)$ as input, and yields $M^{0 \rightarrow 1}$ as output, that is, $M^{0 \rightarrow 1} = G(I^0, I^1, M^0)$. Here, $M^{0 \rightarrow 1}$ represents the set of masks tracked from $M^0 = F(I^0)$ to I^1 . By checking if each mask that was present in M^0 is also present in $M^{0 \rightarrow 1}$, we can determine which object masks in I^0 still exist or have disappeared in I^1 .

The key idea of our zero-shot SCD approach is to apply a reference image r and a query image q instead of consecutive frames (I^0, I^1) to the tracking model G . Although the tracking model traditionally expects consecutive frames (I^0, I^1) for input, we deviate from this convention by providing reference image r and query image q instead. To avoid potential confusion, we rewrite the input and the output of the tracking model as $M^{r \rightarrow q} = G(r, q, M^r)$. By comparing the masks between M^r and $M^{r \rightarrow q}$, we identify object masks that exist at time t_0 but have disappeared at time t_1 , corresponding to the ‘missing’ class in the change detection task. Specifically,

$$M_{missing} = M^r \setminus M^{r \rightarrow q}. \quad (1)$$

Additionally, we run the tracking model G again by reversing the order reference image r and query image q and feed them to G to obtain $M^{q \rightarrow r} = G(q, r, M^q)$. Similarly, we predict the ‘new’ objects by $M_{new} = M^q \setminus M^{q \rightarrow r}$, which represent the objects that appear at time t_1 but were absent at time t_0 . Our pixel-wise prediction is obtained by applying the union of masks within M_{new} and $M_{missing}$. Pixels experiencing both ‘new’ and ‘missing’ occurrences are considered ‘replaced.’ Formally, change prediction $P_{changed}$ is

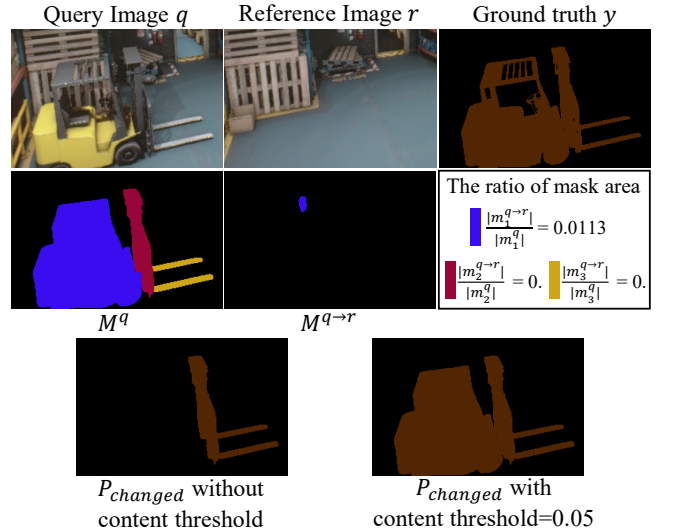


Figure 2: **Illustration of the content threshold.** Since the yellow forklift in q has disappeared in r , all the three masks (blue, red, and yellow masks) in M^q have no associated masks in $M^{q \rightarrow r}$. However, the tracking model creates a small area of the blue mask in $M^{q \rightarrow r}$ due to the content gap. This makes it mistakenly classified as a static object. To address this, we propose a content threshold to filter out masks whose area significantly reduces after tracking.

determined by:

$$\begin{aligned} P_{missing} &= \bigcup M_{missing} \\ P_{new} &= \bigcup M_{new} \\ P_{replaced} &= P_{missing} \cap P_{new} \\ P_{changed} &= P_{missing} \cup P_{new} \end{aligned} \quad (2)$$

The entire process of this approach is illustrated in Figure 1.

Addressing Content Gap and Style Gap

As presented in the previous section, the key idea of our zero-shot SCD approach is to exploit the similarity between SCD and tracking tasks. However, directly applying this concept to various SCD scenarios leads to suboptimal performance due to inherent differences between the two tasks. In this section, we analyze these differences and propose corresponding solutions.

The first difference is the content gap, which refers to abrupt changes in content between the reference and query images. In traditional tracking tasks, objects typically disappear gradually over multiple frames rather than suddenly, and new objects appear gradually over multiple frames, implying that tracking tasks have little content gap. In contrast, SCD involves abrupt changes where objects disappear or appear within a single frame and it has a large content gap. Therefore, when the tracking model G trained on the tracking dataset is directly applied to SCD, the tracking model G tends to create small segments even for objects that have

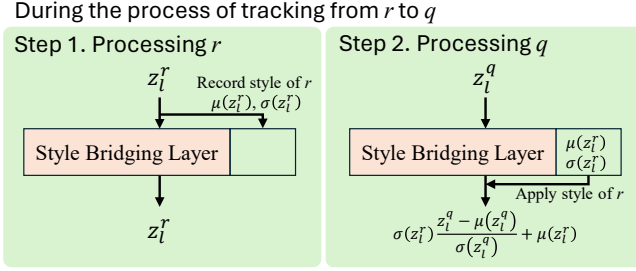


Figure 3: **Illustration of the style bridging layer.** During the processing of the first image, the style is saved while the feature is passed through unchanged. When processing the second image, the saved style is applied to the feature.

disappeared, as shown in Figure 2. In the first row, the yellow forklift in the query image is missing from the reference image, but, in the second row, the mask in $M^{q \rightarrow r}$ tracked from a blue mask in M^q has a small segment. This remaining small segment makes the identification of missing objects very difficult.

To address the content gap, we propose considering an object as disappeared if its size is significantly reduced after tracking, even if it has not completely vanished. To the end, we introduce a content threshold τ and we compare the areas of the masks before and after tracking. If the ratio is less than the content threshold τ , we consider the corresponding object is missing or newly appeared. We define the \setminus^τ operator to replace the \setminus operator in equation 1 as follows, where $|m_i^*|$ denotes the area of the i -th mask in set $*$:

$$A \setminus^\tau B := \{m_i^A \mid \frac{|m_i^B|}{|m_i^A|} < \tau, \quad \forall m_i^A \in A\}. \quad (3)$$

By introducing this operator, we have $M_{missing} = M^r \setminus^\tau M^{r \rightarrow q}$. The value of τ is automatically determined based on the input data. Further details and discussions on the determination of τ are provided in the supplementary material.

The second difference between tracking tasks and SCD is the style gap, which refers to the difference in style between the reference and query images. Change detection data have large temporal gaps, therefore lighting, weather, or season can change. These changes are commonly modeled as style changes (Tang et al. 2023). We define such variations as the style gap, which is not considered in traditional tracking tasks and can thus significantly degrade SCD performance.

To address the style gap, we introduce a style bridging layer (SBL) by incorporating an Adaptive Instance Normalization (AdaIN) layer (Huang and Belongie 2017) into the residual blocks of ResNet backbone (He et al. 2016) of the tracking model G . The AdaIN layer, widely used to reduce style differences between images across various fields (Karras, Laine, and Aila 2019; Wu et al. 2019; Xu et al. 2023), references the first image and applies its style to the second image, thereby reducing the style differences between the two images. Inspired by this, SBL addresses the style gap between two inputs without learning, with two

training-free style parameters. For example, during the process $M^{r \rightarrow q} = G(r, q, M^r)$, the style bridging layer records the mean and variance of each layer in image r and applies these statistics when processing image q . Formally, the style bridging layer updates the feature of z_l^q as follows, where z_l^* denotes the l -th layer feature of image $*$.

$$\tilde{z}_l^q = \sigma(z_l^r) \frac{z_l^q - \mu(z_l^q)}{\sigma(z_l^q)} + \mu(z_l^r). \quad (4)$$

The operation of the proposed style bridging layer is illustrated in Figure 3.

Through these two methods, we effectively and simply address the content gap and style gap. Note that the two improvements are also applied in the process $M^{q \rightarrow r} = G(q, r, M^q)$ and $M_{new} = M^q \setminus^\tau M^{q \rightarrow r}$.

Extension to the Video Sequences

In this subsection, we extend our image-based SCD approach to video sequences. Leveraging video data enhances spatial understanding by capturing scenes from multiple angles. The tracking model in our pipeline allows the seamless extension of our image-based SCD approach to video data.

Consider a video SCD dataset consisting of sequences of reference, query, and change labels, denoted as $\{r^t, q^t, y^t\}_{t=1}^T$, where T represents the length of the video sequence, and t denotes the time index. Compared to the image SCD, the video SCD requires two modifications. The first modification is simply to feed two sequences $\{r^t, q^t\}_{t=1}^T$ instead of image pair $\{r, q\}$ as input to the tracking model. Specifically, we start tracking to detect missing objects in the video with

$$\begin{aligned} M^{r^1 \rightarrow r^2} &= G(r^1, r^2, M^{r^1}) \\ M^{r^1 \rightarrow r^2 \rightarrow q^2} &= G(r^2, q^2, M^{r^1 \rightarrow r^2}), \end{aligned} \quad (5)$$

and continue tracking throughout the entire video with

$$\begin{aligned} M^{r^1 \rightarrow r^t} &= G(r^{t-1}, r^t, M^{r^1 \rightarrow r^{t-1}}) \\ M^{r^1 \rightarrow q^t} &= G(r^t, q^t, M^{r^1 \rightarrow r^t}), \end{aligned} \quad (6)$$

where $M^{r^1 \rightarrow r^t} = M^{r^1 \rightarrow r^2 \rightarrow \dots \rightarrow r^{t-1} \rightarrow r^t}$ and $M^{r^1 \rightarrow q^t} = M^{r^1 \rightarrow r^2 \rightarrow \dots \rightarrow r^{t-1} \rightarrow r^t \rightarrow q^t}$, as shown in Figure 4. In mask formulation, M^X denotes the output from the segmentation model F , whereas $M^{X \rightarrow Y}$ or $M^{X \rightarrow Y}$ denotes the output from tracking model G . This architecture is similar to the structure of the Bayes filters or Markov process (Thrun 2002), in that all the information processed from 1 to $t-1$ are included in $M^{r^1 \rightarrow r^{t-1}}$. Consequently, $M^{r^1 \rightarrow r^t}$ can be incrementally updated from $M^{r^1 \rightarrow r^{t-1}}$ and r^t, q^t , without reprocessing all previous images. During the incremental update from $M^{r^1 \rightarrow r^{t-1}}$ to $M^{r^1 \rightarrow r^t}$, all functions for tracking, including updating feature memory and identifying new objects, are activated. Conversely, during the update from $M^{r^1 \rightarrow r^t}$ to $M^{r^1 \rightarrow q^t}$, these functions are deactivated. This processing sequence is designed to detect ‘missing’ objects, whereas the opposite processing sequence with swapping r and q is employed to detect ‘new’ objects.

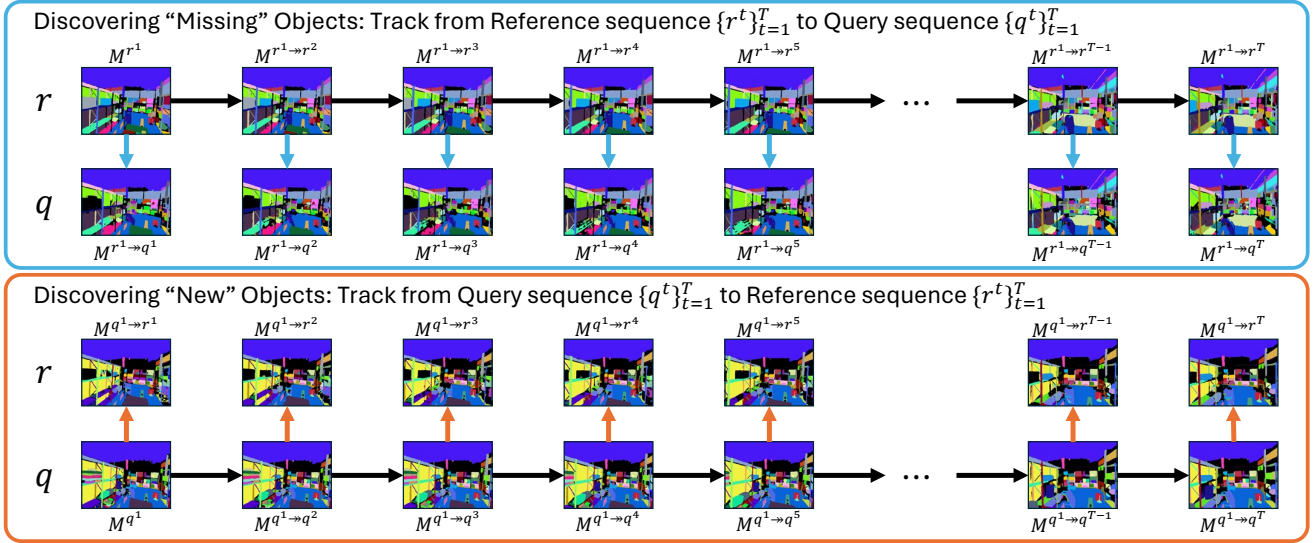


Figure 4: **Zero-shot SCD in video.** We conduct SCD on video sequences by providing sequence pairs instead of image pairs as input to the tracking model G . For each frame, the mask is propagated from the previous frame, resulting in a mask sequence through repeated propagation. SCD in the video is finalized by comparing the mask sequences.

The second modification is redefining $M_{missing}^t$ and M_{new}^t to suit video data. In equation 1, we defined $M_{missing}$ in image SCD as the masks that exist in the reference image r but are absent in the query image q . The definition of $M_{missing}^t$ for video SCD is an extension of this definition to video. Specifically, $M_{missing}^t$ is defined as the masks present in the reference sequence $\{r^t\}_{t=1}^T$ but absent in the query sequence $\{q^t\}_{t=1}^T$. Formally, $M_{missing}^t$ at time index t is defined by:

$$M_{missing}^t = \{M^{r^t} \setminus M^{r^1 \rightarrow q^1}\} \cap \{M^{r^t} \setminus M^{r^1 \rightarrow q^2}\} \cap \dots \cap \{M^{r^t} \setminus M^{r^1 \rightarrow q^T}\}. \quad (7)$$

M_{new}^t is similarly defined with the object that exists in query sequence $\{q^t\}_{t=1}^T$, but is absent in the reference sequence $\{r^t\}_{t=1}^T$.

Through these two extensions, our methodology becomes appropriate for processing videos. According to the definitions of these modifications, the sequence length can range from 1 to infinity. However, we impose an upper bound on the length of a sequence, denoted as T_{max} . If the length of the video exceeds T_{max} , it is divided into multiple sequences, each with a length of T_{max} . The reason for constraining the length of sequences is simple: as sequences lengthen, memory costs increase, while the relevant information for change detection decreases. For instance, in scenarios where the camera is in motion, the initial and final frames of a sequence may capture entirely different locations, rendering them unsuitable for change detection. Conversely, if the camera remains stationary, all frames depict the same scene, and additional frames provide redundant information. Therefore, we ensure more effective SCD by set-

ting the upper bound of the sequence length. For our experiments, we set T_{max} to 60.

Experiments

Experimental Setup

In this section, we briefly introduce the datasets, the relevant settings, and the evaluation metrics.

ChangeSim (Park et al. 2021) is a synthetic dataset with an industrial indoor environment. It includes three subsets with varying environmental conditions: normal, low-illumination, and dusty air. The dataset categorizes changes into four types: new, missing, rotated, and replaced. Despite its variety of environmental variations and change classes, most baseline experiments on this dataset have evaluated only the binary change/unchange classification and have predominantly focused on the normal subset, leaving the dataset’s full potential underexplored. Therefore, we chose the state-of-the-art method, C-3PO (Wang, Gao, and Wang 2023), and reproduced the results under the following conditions: using the original image size (640×480) to fully utilize the rich information; and including all three subsets. Among the four change classes in this dataset, the rotated class, unlike others, involves slight angular changes of the same object rather than complete appearances or disappearances. We considered this as the object remaining static and integrated this class into static for evaluation.

VL-CMU-CD (Alcantarilla et al. 2018) is a dataset that includes information on urban street view changes over a long period, encompassing seasonal variations. Following the baseline approach, we performed predictions using 512×512 -sized images. As the change class in this dataset is limited to a binary classification of the ‘missing’ class, we used only the ‘missing’ class for our three types of prediction.

ChangeSim: In-domain							
Method	Trained Set	Test Set	Static	New	Missing	Replaced	mIoU
C-3PO	Normal	Normal	94.2	14.3	5.3	17.1	32.7
Ours	-		93.9	29.6	12.3	7.3	35.8
C-3PO	Dusty-air	Dusty-air	94.0	9.3	2.8	12.6	29.7
Ours	-		88.6	23.2	6.4	8.1	31.6
C-3PO	Low-illum.	Low-illum.	93.8	5.4	0.6	8.4	27.1
Ours	-		80.6	9.4	4.7	6.3	25.2

Table 1: **Experimental results on ChangeSim.** The results are expressed in per-class IoU and mIoU scores. Despite the absence of a training process, our model outperformed the baseline’s in-domain performance in two out of three subsets.

ChangeSim: Cross-domain				
Method	Trained Set	Test set		
		Normal	Dusty-air	Low-illum.
C-3PO	Normal	32.7	27.2	26.7
	Dusty-air	29.6	29.7	26.9
	Low-illum.	29.4	27.1	27.1
Ours	-	35.8	31.6	25.2

Table 2: **Experimental results on ChangeSim, cross-domain.** The results are expressed in the mIoU score across all change classes. We trained the baseline model on each subset and tested it across all subsets. The experimental results show that the baseline model achieves the highest performance when the training set and test set are the same, while performance degrades when the training and test sets differ. In contrast, our method is free from this issue.

PCD (Sakurada and Okatani 2015) is a dataset consisting of panoramic images and includes two subsets: GSV and TSUNAMI. Following the baselines, we performed predictions on reshaped images of size 256×1024 . Each data point is classified into binary change or unchanged categories. We consider the detected new, missing, and replaced predictions into a ‘changed’ class for evaluation.

Evaluation Metrics Following the previous work, we employ the mean Intersection over Union (mIoU) metric for ChangeSim and F1 score for VL-CMU-CD and PCD datasets.

Experimental Results

Table 1 presents the experimental results with other state-of-the-art, C-3PO (Wang, Gao, and Wang 2023) from ChangeSim. C-3PO is reproduced under the conditions described in the previous section. The baseline model is tested on the same datasets as its training dataset, denoted as in-domain. The table shows that our model achieved superior performance in two out of three subsets: normal and dusty-air, with mIoU of 35.8 and 31.6, respectively. However, our model shows lower performance in low-illumination subset, with mIoU of 25.2.

VL-CMU-CD & PCD				
Method	Trained Set	Test set		
		VL-CMU-CD	PCD	Average
C-3PO	VL-CMU-CD	79.4	11.6	45.5
	PCD	24.3	82.4	53.4
Ours	-	51.6	56.5	54.0

Table 3: **Experimental results on VL-CMU-CD and PCD.** The results are expressed in the F1 score. The baseline model performs best when the training and test are identical. However, its performance significantly declines when these datasets differ. Conversely, our method is robust to changes in the dataset, maintaining performance without the need for retraining whenever the test environment changes.

However, traditional train-based approaches are specialized for the style variation on which they were trained, becoming highly vulnerable when the domains differ. To illustrate this, we conducted additional experiments testing the baseline model on different domains from the ones it was trained on. Specifically, we tested the baseline model trained on a particular subset of ChangeSim on the other subsets, denoted as cross-domain. The experimental results are shown in Table 2. The baseline model, being specialized for their in-domain data, suffers performance drops when the data changes, indicating a lack of generalization. Specifically, when the baseline model trained on the dusty-air subset is tested on the same subset, it achieves a mIoU of 29.7. However, when the model is trained on the normal or low-illumination subsets and tested on the dusty-air subset, the mIoU scores are relatively lower, at 27.2 and 27.1, respectively. This performance drop is also observed in other cross-domain experiments. Conversely, our approach, which is not tailored to any specific style variation within the training dataset, shows robustness to changing the datasets. In other words, our model can be applied to all subsets without the need for retraining each time the environment changes.

We also conducted experiments on two additional real-world datasets, VL-CMU-CD and PCD. The results are summarized in Table 3. These results reveal a pattern consis-

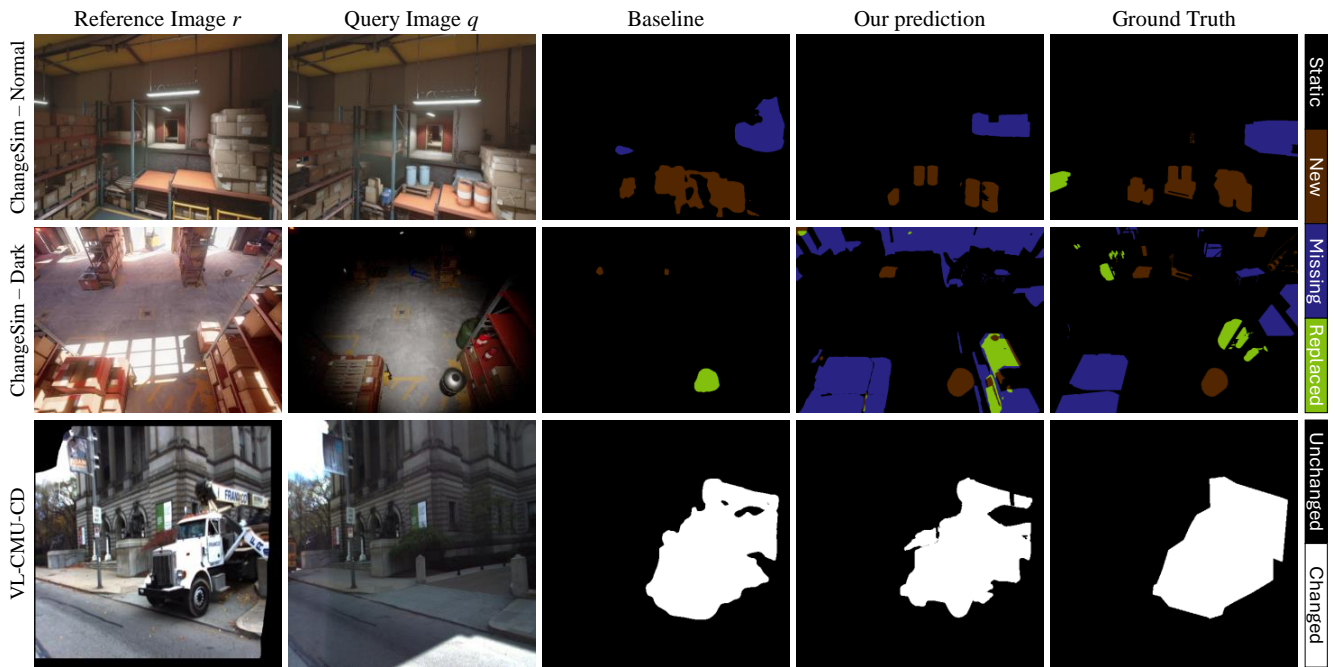


Figure 5: **Qualitative results.** Our approach successfully performs change detection across various datasets without training. For more qualitative results, see the supplementary material.

tent with our previous observations: the baseline model performs well when the training and test datasets are identical, but its performance significantly declines when the datasets differ. In this experiment, the performance drop is particularly severe due to the greater stylistic differences between the datasets. Specifically, the baseline model achieves high in-domain performance with F1 scores of 79.4 and 82.4 on the VL-CMU-CD and PCD datasets, respectively. In contrast, its cross-domain performance drops dramatically to 24.3 and 11.6, respectively. This observation suggests that the baseline model is overfitted to the limited style variations present in the training dataset.

Since the change detection method must function across various seasons and weather conditions in real-world scenarios, robustness to style changes is crucial for reliable performance. The most straightforward way to achieve such robustness against style variations is to employ an approach that does not rely on the training set, as supported by these experimental results.

We present qualitative results in Figure 5. The baseline results correspond to in-domain scenarios, where the training and test datasets are identical. In contrast, our predictions are zero-shot results without any training. The qualitative results show that our approach effectively performs change detection without training. In the supplementary material, we provide more qualitative results and intermediate outcomes of the prediction process.

Ablation Experiments

We conducted extensive ablation experiments and more analyses in the supplementary materials to validate the ef-

ficacy and robustness of our proposed methods. (1) Performance of zero-shot SCD with and without the proposed adaptive content threshold (ACT) and style bridging layer (SBL). (2) Ablation study based on different SBL settings. (3) Ablation study based on different clip lengths. (4) Ablation study based on different ACT settings.

Conclusion

In this paper, we present a novel approach to zero-shot Scene Change Detection (SCD) applicable to both image and video. Our method performs SCD without training by leveraging a tracking model, which inherently performs change detection between consecutive video frames by recognizing common objects and identifying new or missing objects. To adapt the tracking model specifically for SCD, we propose two training-free components: the style bridging layer and the adaptive content threshold. Through extensive experiments on three SCD datasets, our approach demonstrates its versatility by showing its robustness to various environmental changes. We believe that our work offers a fresh perspective on SCD and represents a significant step forward in its practical application.

Acknowledgments

This work was supported by Institute of Information & communications Technology Planning & Evaluation (IITP) grant funded by the Korea government(MSIT) (No.2022-0-01025, Development of core technology for mobile manipulator for 5G edge-based transportation and manipulation)

References

- Agarwal, A.; Kumar, S.; and Singh, D. 2019. Development of neural network based adaptive change detection technique for land terrain monitoring with satellite and drone images. *Defence Science Journal*, 69(5): 474.
- Alcantarilla, P. F.; Stent, S.; Ros, G.; Arroyo, R.; and Gherardi, R. 2018. Street-view change detection with deconvolutional networks. *Autonomous Robots*, 42: 1301–1322.
- Chen, B.; Chen, Z.; Deng, L.; Duan, Y.; and Zhou, J. 2016. Building change detection with RGB-D map generated from UAV images. *Neurocomputing*, 208: 350–364.
- Chen, S.; Yang, K.; and Stiefelwagen, R. 2021. Dr-tanet: Dynamic receptive temporal attention network for street scene change detection. In *2021 IEEE Intelligent Vehicles Symposium (IV)*, 502–509. IEEE.
- Cheng, H. K.; Oh, S. W.; Price, B.; Schwing, A.; and Lee, J.-Y. 2023a. Tracking anything with decoupled video segmentation. In *Proceedings of the IEEE/CVF International Conference on Computer Vision (ICCV)*, 1316–1326.
- Cheng, H. K.; and Schwing, A. G. 2022. Xmem: Long-term video object segmentation with an atkinson-shiffrin memory model. In *European Conference on Computer Vision (ECCV)*, 640–658. Springer.
- Cheng, Y.; Li, L.; Xu, Y.; Li, X.; Yang, Z.; Wang, W.; and Yang, Y. 2023b. Segment and track anything. *arXiv preprint arXiv:2305.06558*.
- Furukawa, Y.; Suzuki, K.; Hamaguchi, R.; Onishi, M.; and Sakurada, K. 2020. Self-supervised Simultaneous Alignment and Change Detection. In *2020 IEEE/RSJ International Conference on Intelligent Robots and Systems (IROS)*, 6025–6031.
- Han, D.; Lee, S. B.; Song, M.; and Cho, J. S. 2021. Change detection in unmanned aerial vehicle images for progress monitoring of road construction. *Buildings*, 11(4): 150.
- He, K.; Zhang, X.; Ren, S.; and Sun, J. 2016. Deep residual learning for image recognition. In *Proceedings of the IEEE Conference on Computer Vision and Pattern Recognition (CVPR)*, 770–778.
- Huang, X.; and Belongie, S. 2017. Arbitrary style transfer in real-time with adaptive instance normalization. In *Proceedings of the IEEE International Conference on Computer Vision (ICCV)*, 1501–1510.
- Jain, S.; Wang, X.; and Gonzalez, J. E. 2019. Accel: A corrective fusion network for efficient semantic segmentation on video. In *Proceedings of the IEEE Conference on Computer Vision and Pattern Recognition*, 8866–8875.
- Karras, T.; Laine, S.; and Aila, T. 2019. A style-based generator architecture for generative adversarial networks. In *Proceedings of the IEEE/CVF Conference on Computer Vision and Pattern Recognition (CVPR)*, 4401–4410.
- Kirillov, A.; Mintun, E.; Ravi, N.; Mao, H.; Rolland, C.; Gustafson, L.; Xiao, T.; Whitehead, S.; Berg, A. C.; Lo, W.-Y.; et al. 2023. Segment anything. In *Proceedings of the IEEE/CVF International Conference on Computer Vision (ICCV)*, 4015–4026.
- Lee, S.; and Kim, J.-H. 2024. Semi-Supervised Scene Change Detection by Distillation From Feature-Metric Alignment. In *Proceedings of the IEEE/CVF Winter Conference on Applications of Computer Vision (WACV)*, 1226–1235.
- Lv, Z.; Huang, H.; Sun, W.; Jia, M.; Benediktsson, J. A.; and Chen, F. 2023. Iterative training sample augmentation for enhancing land cover change detection performance with deep learning neural network. *IEEE Transactions on Neural Networks and Learning Systems*.
- Maquiling, V.; Byrne, S. A.; Niehorster, D. C.; Nyström, M.; and Kasneci, E. 2024. Zero-shot segmentation of eye features using the segment anything model (sam). *Proceedings of the ACM on Computer Graphics and Interactive Techniques*, 7(2): 1–16.
- Park, J.-M.; Jang, J.-H.; Yoo, S.-M.; Lee, S.-K.; Kim, U.-H.; and Kim, J.-H. 2021. Changesim: Towards end-to-end online scene change detection in industrial indoor environments. In *2021 IEEE/RSJ International Conference on Intelligent Robots and Systems (IROS)*, 8578–8585. IEEE.
- Park, J.-M.; Kim, U.-H.; Lee, S.-H.; and Kim, J.-H. 2022. Dual task learning by leveraging both dense correspondence and Mis-correspondence for robust change detection with imperfect matches. In *Proceedings of the IEEE/CVF Conference on Computer Vision and Pattern Recognition (CVPR)*, 13749–13759.
- Peng, Z.; Tian, Q.; Xu, J.; Jin, Y.; Lu, X.; Tan, X.; Xie, Y.; and Ma, L. 2023. Generalized Category Discovery in Semantic Segmentation. *arXiv preprint arXiv:2311.11525*.
- Rajič, F.; Ke, L.; Tai, Y.-W.; Tang, C.-K.; Danelljan, M.; and Yu, F. 2023. Segment anything meets point tracking. *arXiv preprint arXiv:2307.01197*.
- Sachdeva, R.; and Zisserman, A. 2023. The Change You Want to See. In *Proceedings of the IEEE/CVF Winter Conference on Applications of Computer Vision (WACV)*.
- Sakurada, K.; and Okatani, T. 2015. Change detection from a street image pair using cnn features and superpixel segmentation. In *British Machine Vision Conference (BMVC)*.
- Sakurada, K.; Okatani, T.; and Deguchi, K. 2013. Detecting changes in 3D structure of a scene from multi-view images captured by a vehicle-mounted camera. In *Proceedings of the IEEE Conference on Computer Vision and Pattern Recognition (CVPR)*, 137–144.
- Sakurada, K.; Shibuya, M.; and Wang, W. 2020. Weakly supervised silhouette-based semantic scene change detection. In *2020 IEEE International Conference on Robotics and Automation (ICRA)*, 6861–6867. IEEE.
- Seo, M.; Lee, H.; Jeon, Y.; and Seo, J. 2023. Self-pair: Synthesizing changes from single source for object change detection in remote sensing imagery. In *Proceedings of the IEEE/CVF Winter Conference on Applications of Computer Vision (WACV)*, 6374–6383.
- Song, F.; Dan, T.; Yu, R.; Yang, K.; Yang, Y.; Chen, W.; Gao, X.; and Ong, S.-H. 2019. Small UAV-based multi-temporal change detection for monitoring cultivated land cover changes in mountainous terrain. *Remote sensing letters*, 10(6): 573–582.

- Sun, C.; Wu, J.; Chen, H.; and Du, C. 2022. SemiSANet: A semi-supervised high-resolution remote sensing image change detection model using Siamese networks with graph attention. *Remote Sensing*, 14(12): 2801.
- Tang, G.; Ni, J.; Chen, Y.; Cao, W.; and Yang, S. X. 2023. An improved CycleGAN based model for low-light image enhancement. *IEEE Sensors Journal*.
- Thrun, S. 2002. Probabilistic robotics. *Communications of the ACM*, 45(3): 52–57.
- Wang, G.-H.; Gao, B.-B.; and Wang, C. 2023. How to reduce change detection to semantic segmentation. *Pattern Recognition*, 138: 109384.
- Wu, Z.; Wang, X.; Gonzalez, J. E.; Goldstein, T.; and Davis, L. S. 2019. Ace: Adapting to changing environments for semantic segmentation. In *Proceedings of the IEEE/CVF International Conference on Computer Vision (ICCV)*, 2121–2130.
- Xu, Q.; Zhang, R.; Wu, Y.-Y.; Zhang, Y.; Liu, N.; and Wang, Y. 2023. Simde: A simple domain expansion approach for single-source domain generalization. In *Proceedings of the IEEE/CVF Conference on Computer Vision and Pattern Recognition (CVPR)*, 4797–4807.
- Yang, Z.; and Yang, Y. 2022. Decoupling features in hierarchical propagation for video object segmentation. *Advances in Neural Information Processing Systems*, 35: 36324–36336.
- Zhu, X.; Xiong, Y.; Dai, J.; Yuan, L.; and Wei, Y. 2017. Deep feature flow for video recognition. In *Proceedings of the IEEE conference on computer vision and pattern recognition*, 2349–2358.

Supplementary Material of “Zero-Shot Scene Change Detection”

Technical Appendix

Implementation Details

Details on Mask Generation

This section explains how to create a mask for input into the tracking model. We use the Segment Anything Model (SAM) (Kirillov et al. 2023) to generate the mask proposal. We executed SAM’s automatic mask generation pipeline with the parameters set as shown in Table 4.

Hyperparameter	Value
SAM model	vit_h
points_per_side	32
pred_iou_thresh	0.86
stability_score_thresh	0.92
crop_n_layers	1
crop_n_points_downscale_factor	2
min_mask_region_area	100

Table 4: Hyperparameters of SAM.

Meanwhile, the masks generated by SAM exhibit two characteristics that make them unsuitable for our task. First, there are too many small masks. Second, a single pixel can be assigned to multiple masks. These characteristics are problematic because scene change detection (SCD) operates at the object level. Specifically, since the changes occur at the object level, the mask size should correspond to the object level and not be too small. Moreover, each pixel in the image should belong to only one object, meaning it must belong to at most one mask. Therefore, we conducted the post-processing steps outlined in Table 5. This process ensures that each pixel belongs to at most one mask, and small masks are naturally removed.

Details on Tracking Model

We use DEVA (Cheng et al. 2023a) for our tracking model. We used the DEVA structure with only one modification, incorporating style bridging layers (SBL) within the encoder architecture. The first SBL is positioned immediately after the first convolutional layer, while subsequent SBLs are placed after the addition operation within each residual block (He et al. 2016). DEVA parameters were set as shown in Table 6.

Step	Details
1	Run the Segment Anything Model (SAM) to obtain masks.
2	Sort the SAM masks from smallest to largest area.
3	Overlay the sorted masks in order. This process ensures that if one pixel belongs to multiple masks, the largest mask among them is selected.
4	For each mask, if the ratio of the area covered by the overlaid mask is more than 50%, it is merged with the largest mask among the overlaid masks. This process removes the masks that occluded most of the area through step 3.
5	For the VL-CMU-CD (Alcantarilla et al. 2018) dataset, remove the masks that do not contain any information. These are the black areas at the edges of the images.

Table 5: Mask generation process.

Notably, the extension to video with G reduces the need to run the segmentation model F for every frame and reduces total computation cost. This is based on the observation that most tracking models exploit the similarity between adjacent frames in a video to reduce computation: instead of performing computationally intensive operations on all frames, these operations are restricted to keyframes, while intermediate frames are processed through lightweight feature propagation (Zhu et al. 2017; Jain, Wang, and Gonzalez 2019).

In our experiments, F is executed every 5 frames to get the set of object masks (denoted as `detection_every` in Table 6), while other frames are propagated by G from the previous frame.

Hyperparameter	Value
<code>detection_every</code>	5
<code>voting_frames</code>	3
<code>max_missed_detection_count</code>	5
<code>max_num_objects</code>	200

Table 6: Hyperparameters of DEVA.

Details on Adaptive Content Threshold

The set of missing object masks $M_{missing}^t$ defined by equation 7 in the main paper, are the masks that exist in the reference frame but are missing in the query sequence. If an object mask is detected in any frame of the query sequence, it is not classified as missing. Notably, even if an object mask is absent in the majority of frames within the query sequence, the detection of the object mask in just a single frame prevents it from being classified as missing. As a result, as the number of sequences being compared increases, the model becomes more vulnerable to noise, thereby complicating the accurate prediction of missing objects.

Therefore, we hypothesized that the content threshold should adapt to the length of the video sequence. For the reasons mentioned above, a high content threshold risks missing too many true positives in short sequences, while a low content threshold becomes vulnerable to noise in long sequences. To resolve this trade-off, we designed the adaptive content threshold as a parameter explicitly dependent on the video sequence length.

Specifically, we designed the adaptive content threshold to satisfy the following conditions: (1) It should increase as the clip length gets longer. (2) It should have a lower bound to ensure functionality at the image level. (3) It should have an upper bound to prevent excessive growth. Based on these considerations, we derived a simple equation for the adaptive content threshold that depends solely on the sequence length as follows:

$$\tau = 0.5 - \frac{0.9}{\sqrt{length} + 1}. \quad (8)$$

The effectiveness of this adaptive content threshold is further examined in our ablation studies.

Computing Infrastructure

The experiments were conducted using the Intel Xeon Gold 6426Y CPU and a single NVIDIA RTX A5000 GPU. The software stack employed includes PyTorch 2.1.2 with CUDA version 12.1. The size of memory usage is below 24 GB.

Ablation Experiments

We conducted ablation experiments to show the effectiveness of our approach. All experiments were conducted on the ChangeSim dataset (Park et al. 2021). To conserve space in the tables, the names of each subset are abbreviated: dusty-air is abbreviated as ‘Dust’, and low-illumination as ‘Dark’.

Addressing Content Gap and Style Gap

We evaluate the effectiveness of the proposed adaptive content threshold (ACT) and style bridging layer (SBL). As shown in Table 7, experimental results indicate that the combined use of ACT and SBL yields the highest average performance. Additionally, these experiments offer interesting observations: (1) SBL is effective when the style of reference and query image differ (i.e., dusty-air and low-illumination subset), but its effectiveness diminishes in subsets with consistent styles (i.e., normal subset). (2) ACT demonstrates its

efficacy particularly when the model’s tracking performance is high (e.g., normal subset). In experiments where tracking performance is poor (e.g., low-illumination subset), the addition of ACT leads to a decline in performance.

Config.		ChangeSim			
ACT	SBL	Normal	Dust	Dark	Average
		28.2	24.4	25.0	25.9
	✓	27.1	27.0	25.7	26.6
✓		36.0	18.1	21.6	25.3
✓	✓	35.8	31.6	25.2	30.9

Table 7: Ablation study on ACT and SBL.

The Number of SBL

We experiment to determine the optimal number of SBL required. We progressively add SBL from the early layer of the encoder. The first Style Bridging Layer (SBL) was placed directly after the first convolutional layer, and the following SBLs were inserted after the addition operation within each residual block. The experimental results are shown in Table 8. The experimental results indicate that applying SBL to all encoder blocks yields the best performance.

# of SBL	ChangeSim			
	Normal	Dust	Dark	Average
0	36.0	18.1	21.6	25.3
1	35.7	29.2	23.9	29.6
2	36.1	31.1	24.7	30.6
3	36.0	31.5	25.0	30.8
4	35.8	31.6	25.2	30.9

Table 8: Ablation study on the number of SBL.

The Length of Sequence

We conduct experiments under various T_{max} values. As shown in Table 9, our method shows a significant improvement when extended to video compared to the image-based SCD approach ($T_{max} = 1$). However, it is notable that increasing T_{max} does not consistently lead to improved performance; increasing the video length beyond 60 has little to no impact on performance or may even lead to a decline.

T_{max}	ChangeSim			
	Normal	Dust	Dark	Average
1	33.6	28.9	22.2	28.2
30	35.6	31.6	24.4	30.5
60	35.8	31.6	25.2	30.9
90	35.6	31.2	25.6	30.8
unlimited	33.3	30.5	25.6	29.8

Table 9: Ablation study on the length of the sequence T_{max} .

The Adaptive Content Threshold

To illustrate the necessity of varying the content threshold according to the sequence length, we conducted experiments across three different sequence lengths. The three sequence lengths were 1, 60, and 30, which are the T_{max} for image-level SCD, our standard T_{max} for video, and the intermediate value, respectively. The fixed threshold values were set to 0.05 and 0.4, approximating the values of ACT when $T_{max} = 1$ and $T_{max} = 60$, respectively.

As shown in Table 10, when the sequence length is 1, a threshold of 0.05 performs the best, while performance is poor at a threshold of 0.4. Conversely, for sequence lengths of 30 and 60, a threshold of 0.05 results in the lowest performance, while higher thresholds improve performance. Furthermore, the results indicate that the ACT consistently achieves the best performance across all sequence lengths. This shows the validity and effectiveness of ACT and supports the argument that the threshold should be influenced by the sequence length.

T_{max}	τ	ChangeSim			
		Normal	Dust	Dark	Average
1	0.05	33.6	28.9	22.2	28.2
	0.4	31.9	24.6	18.4	25.0
	Adaptive	33.6	28.9	22.2	28.2
30	0.05	31.1	29.9	26.2	29.1
	0.4	35.4	31.3	23.9	30.2
	Adaptive	35.6	31.6	24.4	30.5
60	0.05	30.0	29.0	26.5	28.5
	0.4	35.8	31.5	25.2	30.8
	Adaptive	35.8	31.6	25.2	30.9

Table 10: Ablation study on the content threshold (τ).

Qualitative Results

We present additional qualitative results in Figures 6, 7, 8, and 9 to show the effectiveness of our approach across various datasets. To enhance understanding, detailed images of the intermediate processes are also provided. During the intermediate process, identical masks before and after tracking are represented by the same color. Specifically, the same colored masks in M^r and $M^{r \rightarrow q}$ denote the same object mask, and the same applies to M^q and $M^{q \rightarrow r}$. However, since M^r and M^q do not share a tracking relationship, the same color between these two images holds no relationship.

The qualitative results show that our approach effectively identifies new and missing objects, and generates the final prediction accurately.

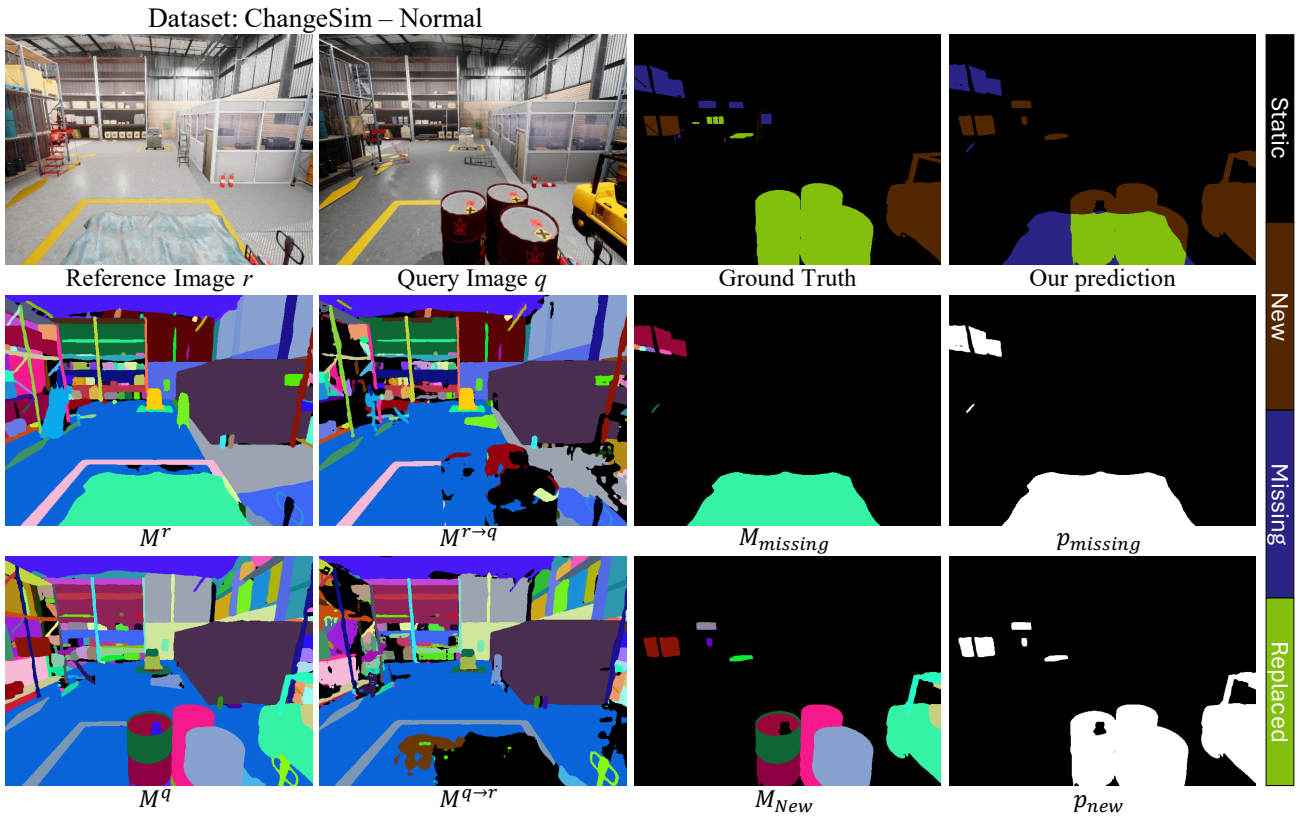
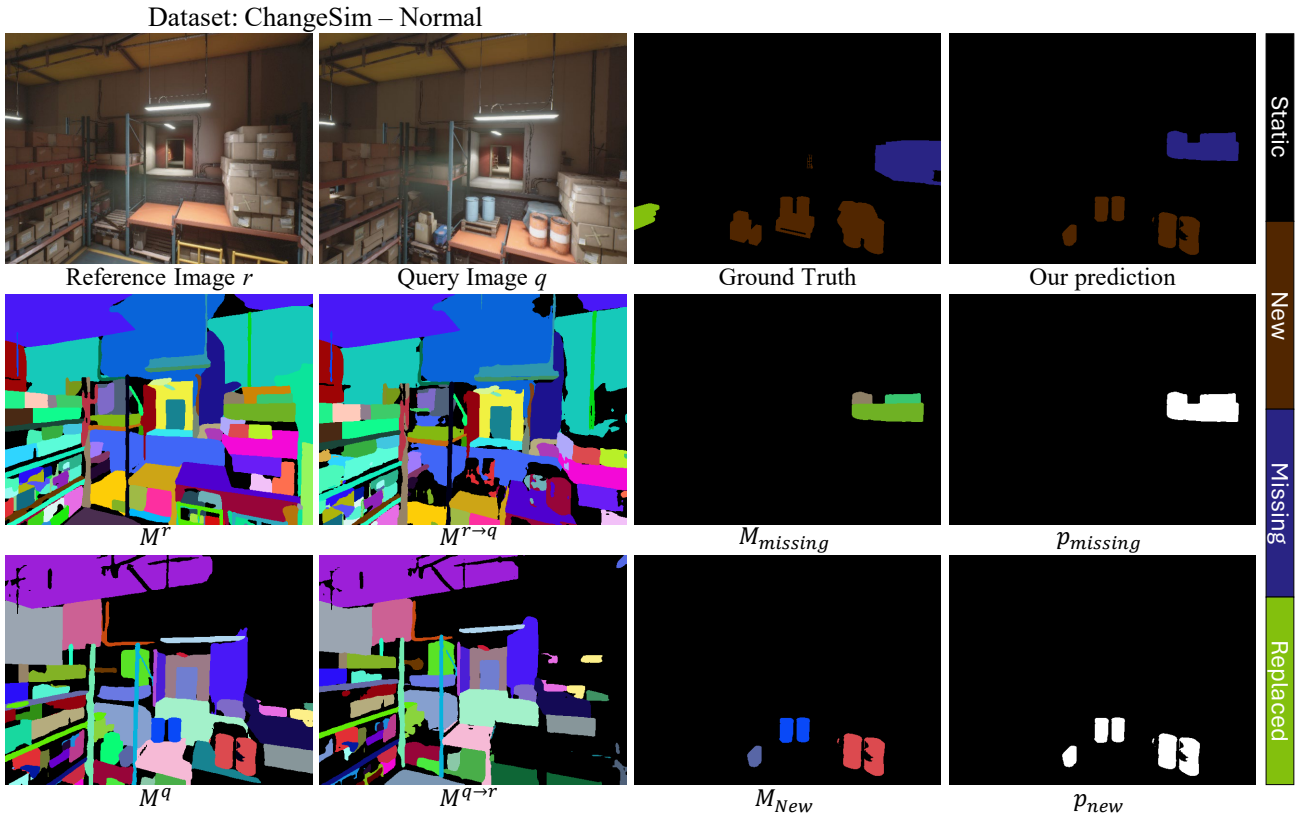


Figure 6: Qualitative results on ChangeSim Normal subset.

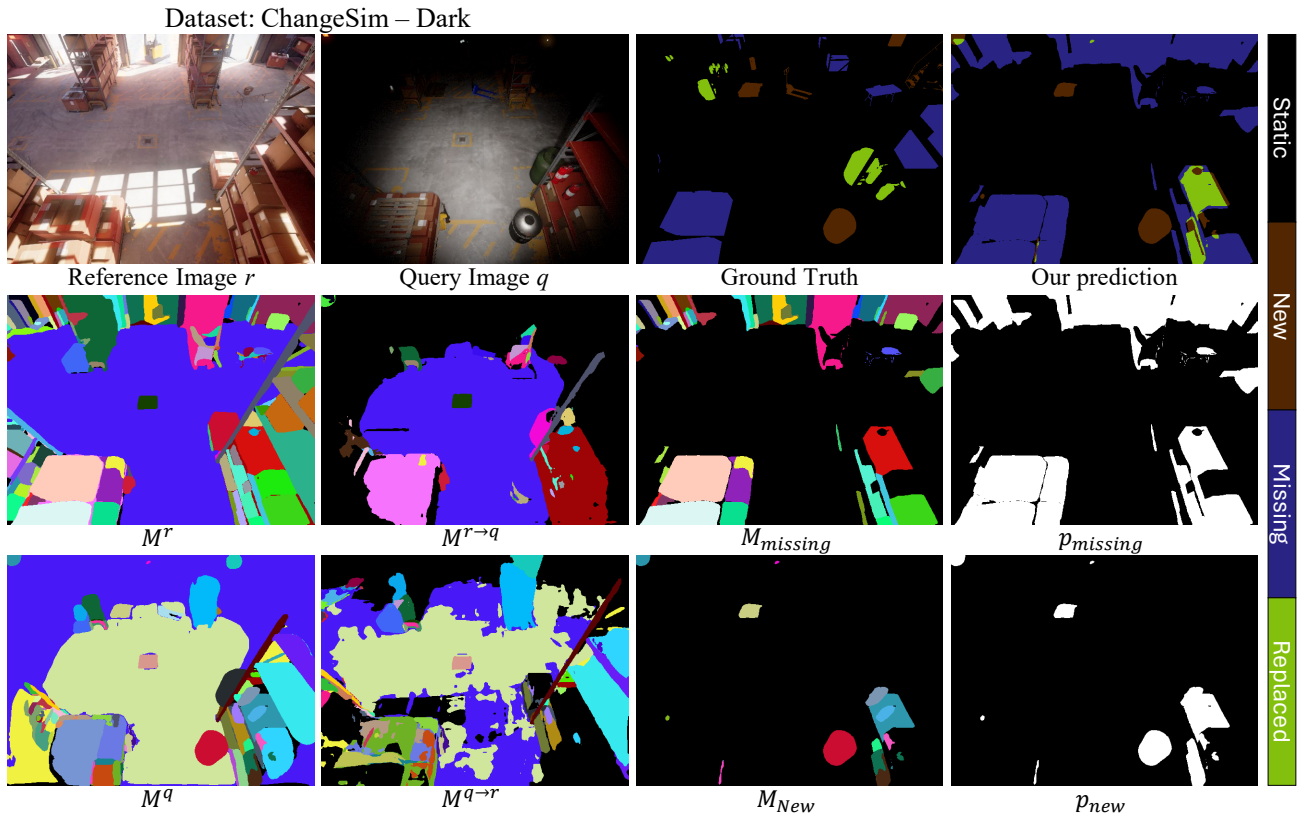
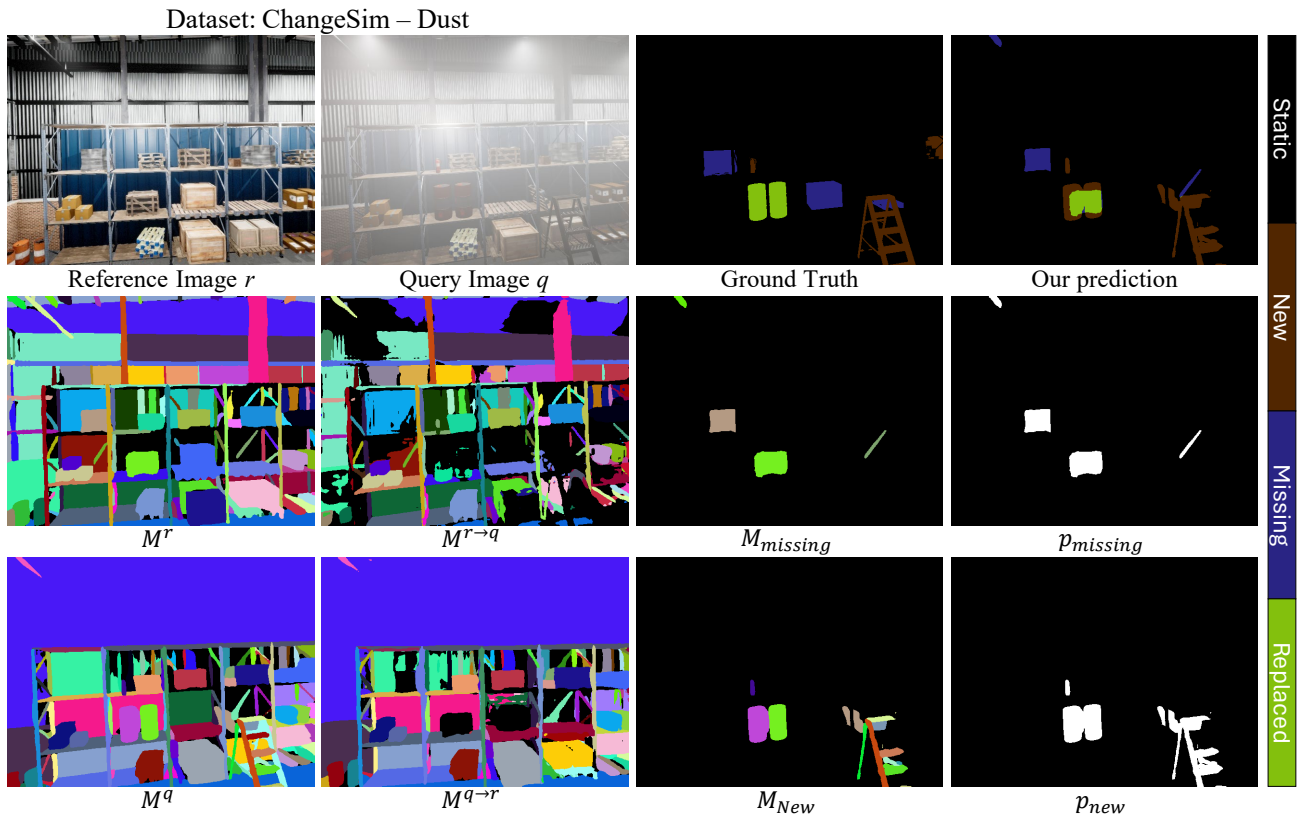
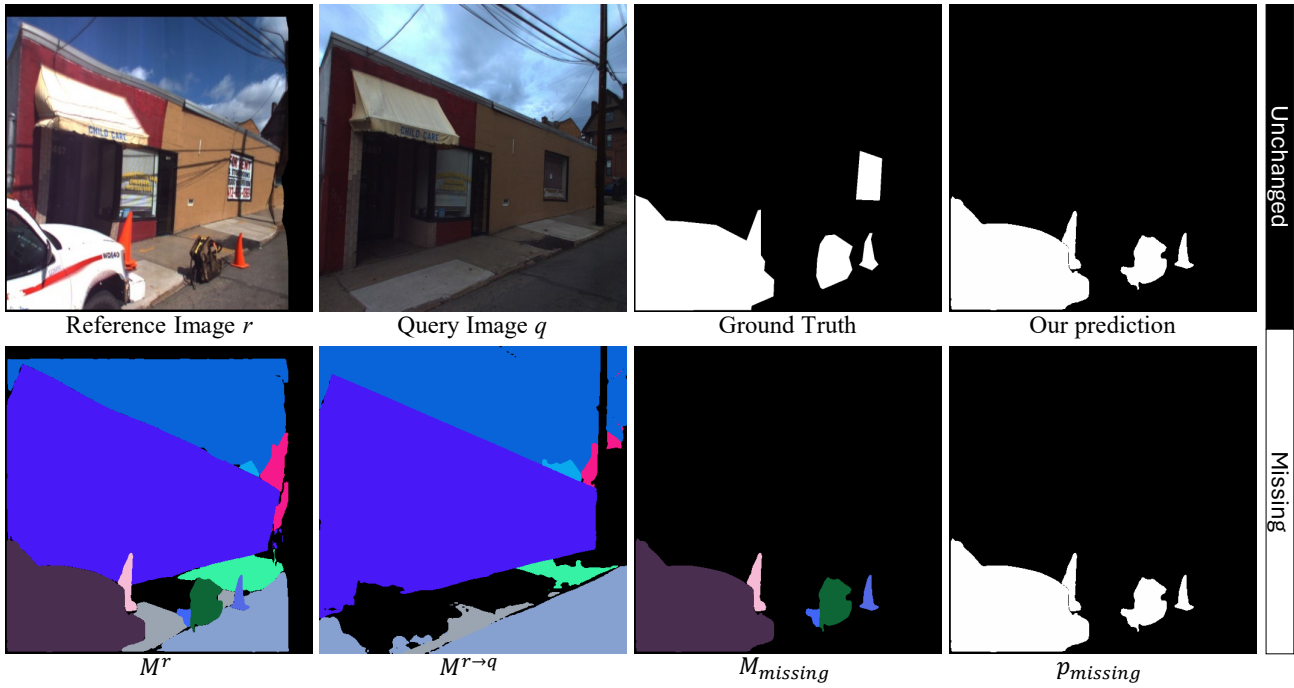


Figure 7: Qualitative results on ChangeSim Low-illumination and ChangeSim Dusty-air.

Dataset: VL-CMU-CD



Dataset: VL-CMU-CD

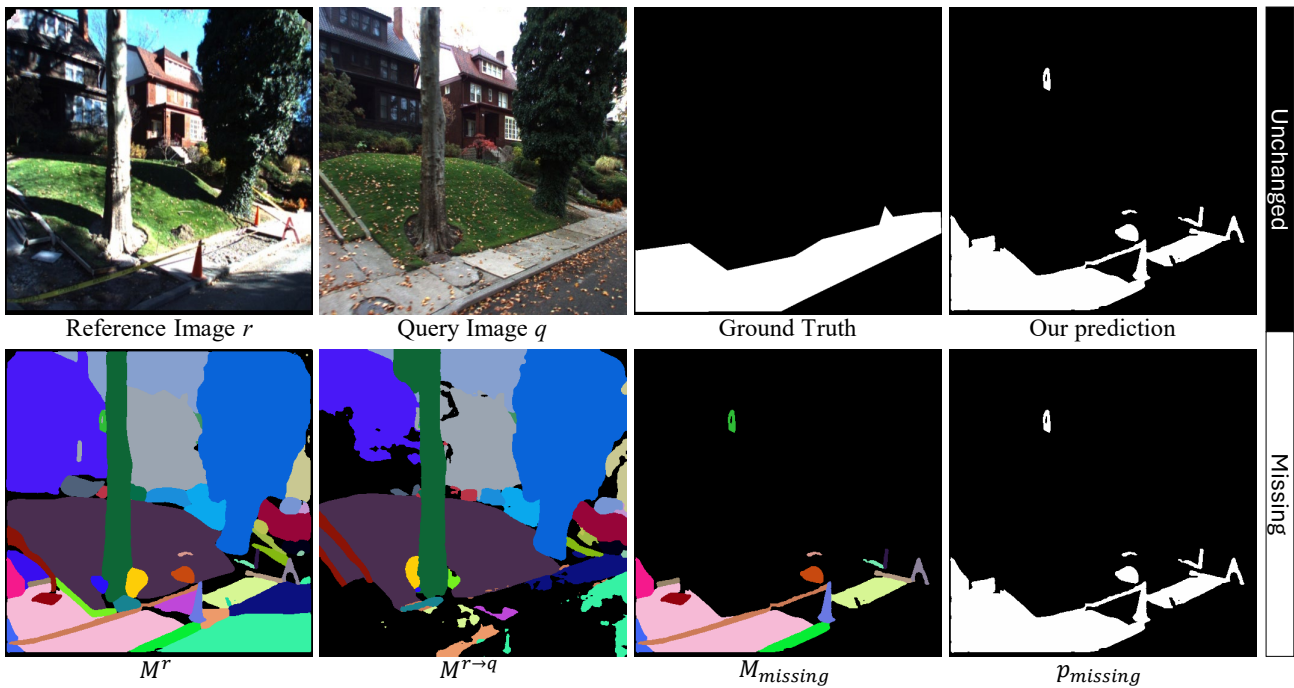


Figure 8: Qualitative results on VL-CMU-CD (Alcantarilla et al. 2018).

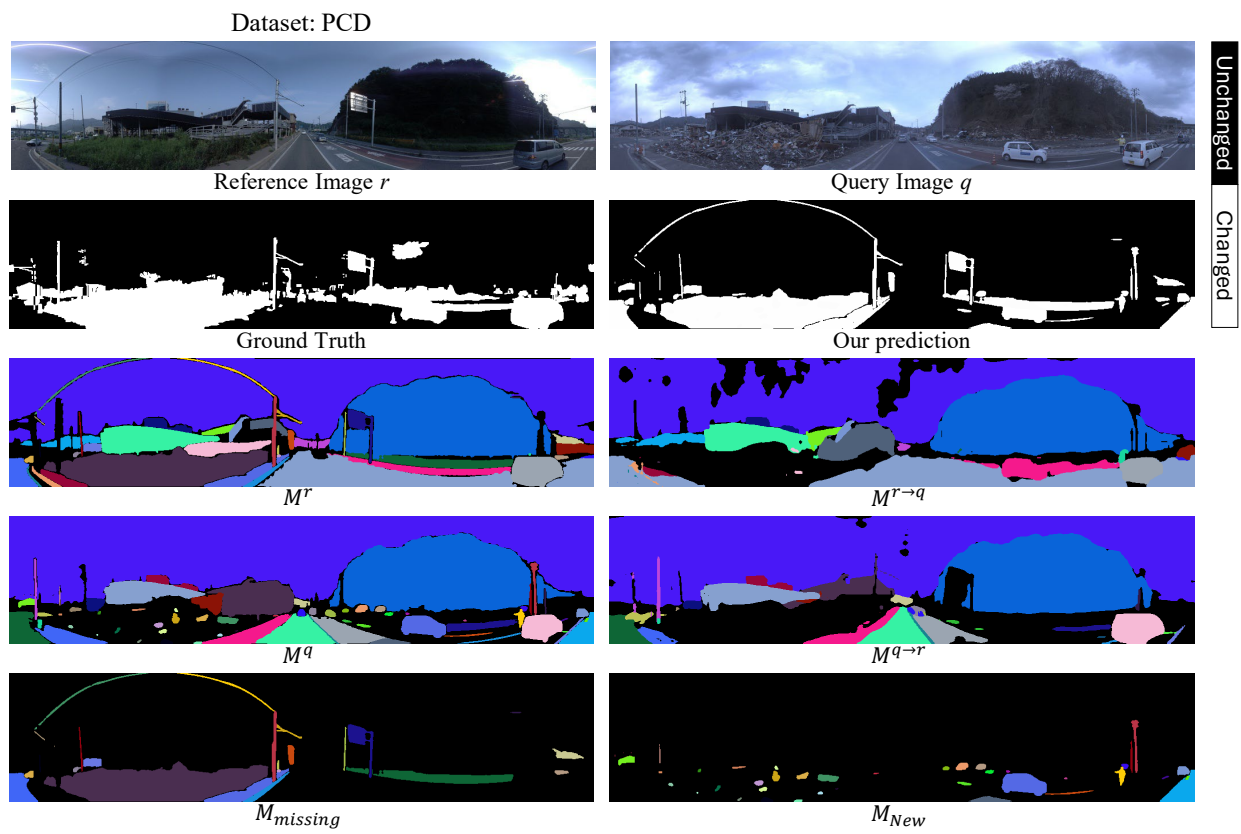
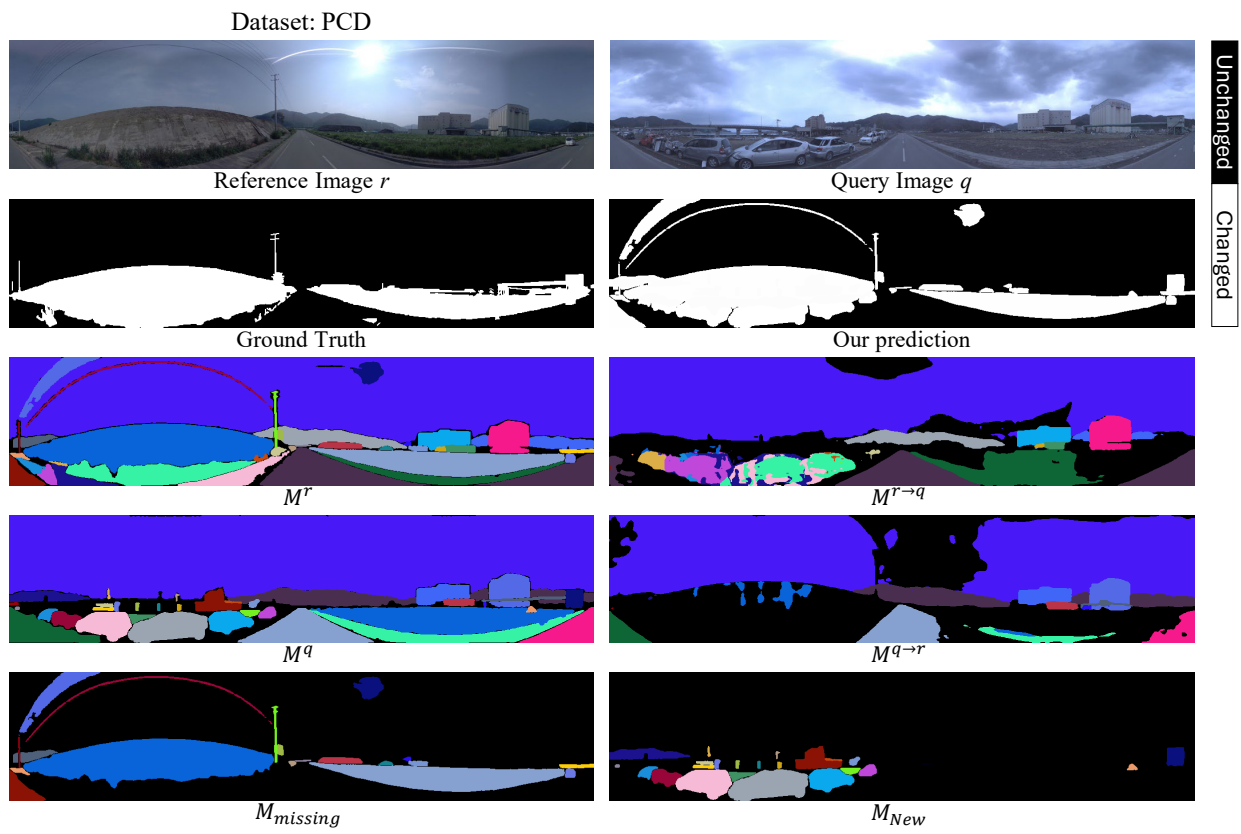


Figure 9: Qualitative results on PCD (Sakurada and Okatani 2015).